Journal of Polymers and the Environment (2024) 32:4405–4421
https://doi.org/10.1007/s10924-024-03220-w

ORIGINAL PAPER

Unveiling the Potential of *Borassus flabellifer's* Leaves Derived ZnO Nanoparticles in Augmenting the Attributes of PLA-Surface Modified Nanocellulose Bio-composite

Pradnya Ghalsasi[1] · Pavada Madhusudan Rao[1] · S. Sruthi[1] · V. S. Avanthi[1] · P. Radha[1]

Accepted: 17 February 2024 / Published online: 1 April 2024

Abstract
The utilization of synthetic plastics has resulted in environmental and human health concerns. Consequently, there is a growing focus on developing eco-friendly alternatives like polylactic acid (PLA). Nonetheless, its drawbacks include slow crystallization, vulnerability to UV radiation, and absence of antibacterial properties. One potential strategy involves integrating nano-cellulose (NC) and metal oxide nanoparticles into PLA to enhance its antibacterial features and mechanical robustness. The NC was extracted from the leaves of *Borassus flabellifer* and further treated with lactic acid to obtain surface-modified NC (SMNC). Besides, the Zinc oxide nanoparticles (ZnO NPs) were green-synthesized using the *B. flabellifer* leaves extract and further characterized through various analytical techniques such as SEM, XRD, and FTIR. The optimized bio-composite ratio was 89.5 mg of PLA, 3.5% (w% of PLA) of SMNC, and 7% (wt% of PLA) of ZnO NPs based on the appearance, water contact angle (WCA), and antimicrobial activities of the bio-composite film. The PLA-SMNC-ZnO NPs film was further characterized and compared with PLA and PLA-SMNC films for its structural, mechanical, and thermal properties. The PLA-SMNC- ZnO NPs film exhibited an improved tensile strength of 13.9 MPa and Young's modulus of 0.00689 GPa than PLA and PLA-SMNC. Also, the thermal stability of PLA-SMNC-ZnO NPs film was 320 °C from TGA. Additionally, PLA-SMNC- ZnO NPs film exhibited reduced water absorption and improved resistance to UV radiation. In conclusion, these findings validate the potential of the ZnO NPs derived from *B. flabellifer's* leaves in improving the versatility of PLA.

✉ P. Radha
radhap@srmist.edu.in

[1] Bioprocess and Bioseparation Laboratory, Department of Biotechnology, College of Engineering and Technology, SRM Institute of Science and Technology, Kattankulathur, Chengalpattu District, Tamil Nadu 603203, India

Graphical Abstract

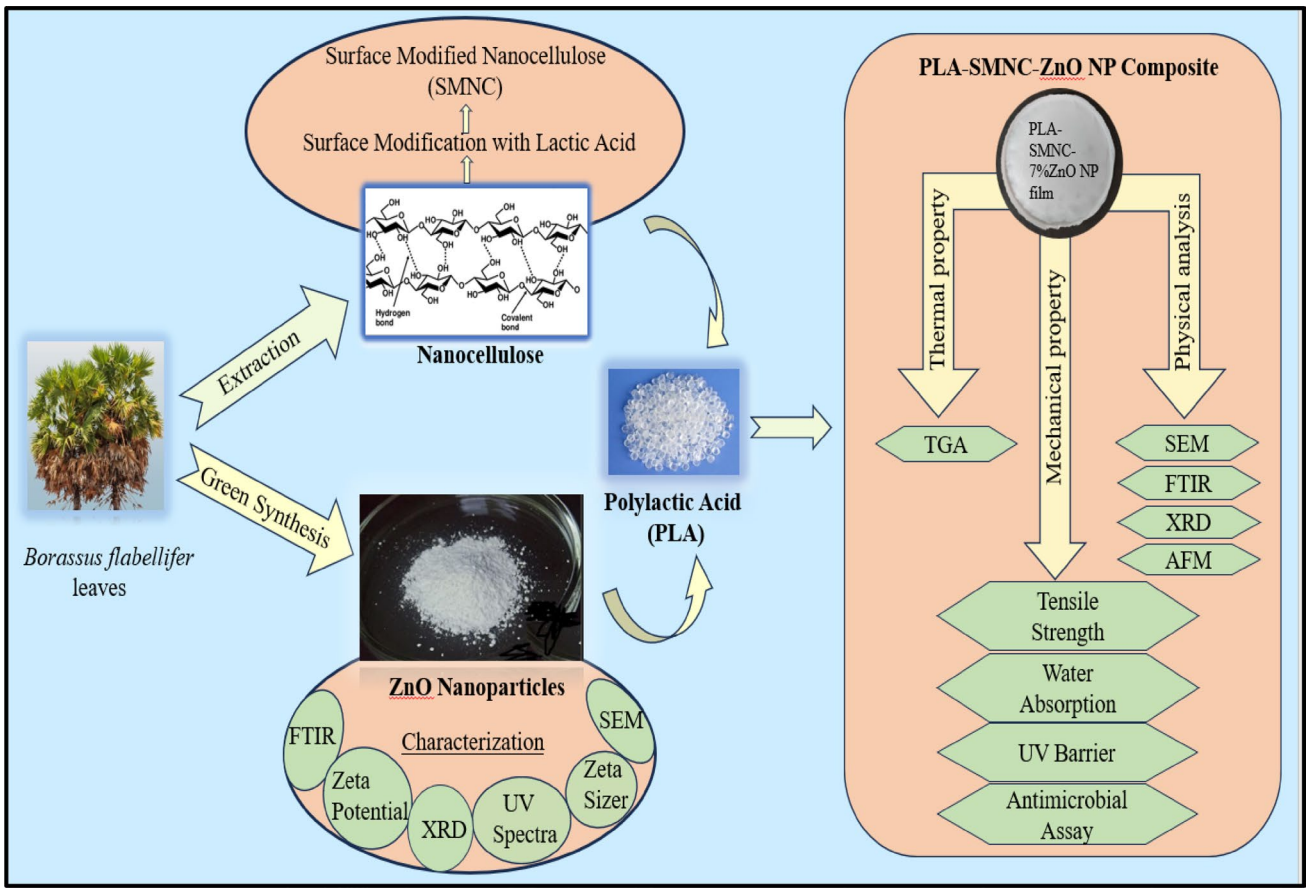

Keywords Polylactic acid · *Borassus flabellifer* · Green synthesis · Zinc oxide nanoparticles · Surface-modified nanocellulose

Introduction

Reducing dependency on conventional plastics while pursuing environment-friendly alternatives is critical in an increasingly eco-conscious world. Societies may promote a more sustainable future and mitigate the negative effects of conventional plastics on the environment by using biodegradable materials. Switching to "green" materials is essential since traditional plastics have a detrimental effect on the environment [1]. One of the most promising solutions is the creation and widespread use of biodegradable substances. These substances minimize the adverse effects of non-biodegradable plastics, such as pollution and resource depletion. As a result, biopolymers are being used as a practical substitute for plastics derived from petroleum [2, 3]. These biopolymers have several benefits over conventional plastics since they are made from sustainable biomass sources like maize, starch, and vegetable oil [4]. Primarily, biopolymers can consistently degrade over time owing to the action of microbes. This has an immense advantage since it lessens the number of plastic debris that ends up in landfills and ecosystems. Moreover, they can be developed to have good barrier properties against oxygen and moisture [5], preserving food products' freshness and shelf life. Biopolymers such as polyhydroxybutyrate (PHB), polylactic acid (PLA), polycaprolactone (PCL), starch, cellulose, chitosan, etc., have been utilized in food packaging [6]. One of the most widely used bio-based and biodegradable polymers for food packaging is PLA which is recognized for having mechanical properties equivalent to polymers based on petroleum like polyethylene and polypropylene [7]. Furthermore, PLA is considered to be "generally recognized as safe" (GRAS) [8], which confirms its suitability in food packaging applications. However, pure PLA film is too brittle to be employed as a thin film and has no antibacterial and antioxidant properties [9, 10].

Nanofillers, such as cellulose, lignin, clay, TiO_2, graphene, calcium carbonate silica, etc., have been blended with the PLA to enhance the mechanical and thermal characteristics of PLA [11–13]. *Borassus flabellifer* is a versatile tree that belongs to the *Arecaceae* family and is widely distributed in the southern region of the Indian subcontinent. The proximate analysis of the *B. flabellifer* leaves exposed the high content of cellulose. The *B. flabellifer* leaves derived nanocellulose (NC) were reported for their excellent mechanical properties, such as high tensile strength, stiffness, and UV stability when blending with the PLA matrix as a nanofiller [11, 14, 15]. However, NC's hydrophilic properties make distributing it evenly in the hydrophobic PLA matrix difficult. Its usefulness as a reinforcing material is hampered by hydroxyl groups on the NC surface, making it challenging to scatter uniformly in a nonpolar liquid. Therefore, before being further incorporated into PLA, NC is surface-modified by acetylation or transesterification to improve its hydrophobicity [15, 16]. Hence, the PLA matrix has been incorporated with surface-modified nanocellulose (SMNC) to inherit salient features like high surface area-to-volume ratio, enhanced mechanical qualities, and biocompatibility. However, PLA-SMNC composite should possess substantial antimicrobial activity to improve its candidature for widespread use. Various chemical functionalizations with antibacterial groups or blends with metal nanoparticles (NPs) and metal oxides can demonstrate the antibacterial activity of NC [17, 18]. Noble metallic NPs like Au, Ag, Pt, Pd, etc., and non-metallic oxides like ZnO and TiO_2 possess extensive antibacterial and photocatalytic activity [19, 20]. In addition, zinc oxide nanoparticles (ZnO NPs) possess strong UV absorption capability, photocatalytic activity and good stability [19–21]. Moreover, ZnO NPs are cheap and also easy to synthesize. Precipitation, thermal breakdown, hydrothermal synthesis, and physical vapor synthesis are some of the synthesis techniques used to produce ZnO NPs [21–23].

The distinguishing features of our study extend beyond the green synthesis of ZnO alone, with a primary focus on the uniqueness featured in the PLA-SMNC-ZnO NPs film. Foremost, the synchronized utilization of *B. flabellifer* leaves for NC and eco-friendly green synthesis of ZnO NPs by valorizing its extract establishes an unprecedented harmony between these components, addressing inherent compatibility issues in PLA composites. This green synthesis not only contributes to the ecological integrity of the process but also imparts a heightened degree of safety to the ZnO component, aligning seamlessly with stringent standards for various applications. This integrated approach not only streamlines production but also ensures a synergistic interaction within the PLA matrix. The resulting PLA-SMNC-ZnO NP film, characterized comprehensively for its structural, mechanical, and antimicrobial attributes, signifies a breakthrough in the realm of functional biopolymer composites, underpinned by a multifaceted approach to sustainability and innovation.

Materials and Methodology

Green Synthesis of ZnO NPs

The *B. flabellifer* leaves were collected from a local site. These leaves were washed multiple times with purified water to eliminate any impurities. Subsequently, they were gently dried in a controlled hot air oven at 37–40 °C. The dried leaves were carefully processed into a fine powder using ball milling. 5 g of the dried powder was measured and placed into a 250 ml beaker; then, 100 ml of deionized water was added to the beaker and was heated in a water bath for 1 h, maintaining a temperature of 80 °C. The solution was filtered using Whatman No. 1 filter paper, and the resulting extract was carefully collected into another beaker.

Once cooled, this extract was stored for the subsequent green synthesis of ZnO NPs [24]. In a beaker, 0.1 M Zinc Nitrate was dissolved in 100 ml of distilled water and mixed with 20 ml of leaf extract to attain a 5:1 ratio. The pH of the solution was carefully adjusted to the desired range of 10–12 by adding 0.1 M NaOH. The mixture was placed on a magnetic stirrer and stirred at 1000 rpm for 2 h at 60 °C, and afterwards, the mixture was kept at 40 °C for 2 h. After cooling, the sample was sonicated for an hour before being centrifuged at 5000 rpm for 15 min. The supernatant was discarded, and the remaining pellet was washed with distilled water before being centrifuged at the same speed. The pellet was calcinated in a muffle furnace at 400 °C for 3 h [25, 26].

Characterization of ZnO NPs

UV–Visible Spectroscopy

The optical properties and conformation of ZnO NPs were determined using a UV−Vis Spectrophotometer, Agilent Technologies. The sample was prepared by diluting the dried ZnO NPs with water, and distilled water was kept as blank for reference. The spectral analysis was performed within a wavelength of 200–800 nm [27].

Scanning Electron Microscopy (SEM)

SEM is widely used to examine the microstructure and chemistry of various materials. The surface morphology of nanoparticles was studied using Hi-Resolution SEM (Thermoscientific Apreo S). The structure of nanoparticles was observed operating at a voltage of 20 kV.

Fourier Transform Infrared Spectroscopy (FTIR)

FTIR spectroscopy relies on the absorption of infrared radiation when passing through a sample. The Agilent Technologies Cary 600 Series FTIR spectrophotometer was utilized to unravel the distinct characteristics of functional groups present in the ZnO NPs. The recorded spectrum of the powdered sample was examined using the KBr pellet method over a broad wavelength range (400–4000 cm^{-1}), which identifies and differentiates between various molecules based on their unique molecular structures [27].

X-ray Diffraction (XRD)

The X-ray diffractogram (BRUKER USA D8 Advance) was used to examine the powdered ZnO NPs, using monochromatic Cu Ka radiation (1.5419Å) at a voltage of 40 kV and a current of 15mA [28]. By accounting for all possible sample orientations, 2θ angles were obtained. These angles were then converted to d-spacings, enabling the definite recognition of the material. The crystalline size (D) of the synthesized ZnO NPs was estimated using the Debye–Scherrer formula shown below:

$$D = \frac{k\lambda}{\beta coscos\theta} \quad (1)$$

where λ is the X-ray wavelength of 1.5419 Å, k (value 0.9) is the shape factor (dimensionless), θ is the Bragg angle in radians, and β is the full width at half maximum (FWHM) in radian.

Zeta Potential

Utilizing a zeta potential analyzer (Malvern/Nano ZS-90), the zeta potential of the nanoparticles was also measured. The zeta potential could be accurately determined by observing the direction and velocity of the particles in a known electric field. To assess the charge of the nanoparticles, the dried ZnO NPs were first diluted in water, which was later used to obtain accurate and reliable data on the particles [29].

Optimization of Blending Ratio of Bio-composite

PLA (Green biostar P 1006), commercially available, was dissolved in chloroform and heated at 40–60 °C for 15–20 min. NC was extracted from the dried leaves of *B. flabellifer* as described by Arun et al. [30] and surface-modified with lactic acid (LA). The aqueous solution of NC was blended with LA at a 15:1 ratio and 100 g of Stannous chloride ($SnCl_2$). $SnCl_2$ is employed as a catalyst that facilitates the condensation of acid or acyl anhydrides with a cellulosic alcohol group, creating ester bonds (C–O=O), during surface modification of nanocellulose [16]. Further, the solution was homogenized for 10 min at 5000 rpm, followed by ultrasonication for 1 h at 20% amplitude with a pulse of 10 s on and off. The treated NC was kept at 80 °C for 10 h. Afterwards, the surface-modified NC (SMNC) solution was filtered and dried [31]. The quantity of SMNC was kept constant at 3.5% (w/w) of the PLA in the composite preparation, which was optimized in our preliminary studies (data not shown). Varying concentrations of ZnO NPs (ranging from 1 to 7% (w/w) of the PLA) were added into separate beakers and were mixed thoroughly for 10 min. After reheating, the solution was poured onto a plate and left to air dry. The prepared film was analyzed further for various properties [32, 33].

Water Contact Angle Measurement (WCA)

The sessile drop method was used to calculate the different concentrations of PLA-SMNC-ZnO NPs composite film's WCA. A 1 µL water droplet was deposited on the film surface to find the contact angle, and the angle between the droplet and the surface was measured [34].

Antimicrobial Assay

The antibacterial properties of the PLA-SMNC-ZnO NPs biocomposite films were evaluated using the agar diffusion method. A culture of Gram(− ve) *Escherichia coli* (ATCC8739) and Gram(+ ve) *Staphylococcus aureus* (ATCC6538) was prepared by inoculating a loop of bacterial culture into 250 ml of LB media and allowing it to grow overnight in a rotatory shaker at140 rpm. Subsequently, 10 µL of the bacterial dilution was evenly spread on agar petri plates, and wells were created in the solid culture medium. The biocomposite films were then carefully placed in the wells, and Streptomycin discs were employed as the standard control. The plates were subsequently incubated for 24 h at 37 °C to facilitate bacterial growth and the development of inhibition zones around the films. The diameter of the inhibition zone around each film was measured, with a larger diameter indicating a greater extent of bacterial inhibition and stronger antibacterial activity [35]. Based on WCA measurement and antimicrobial assay, it was found that 7% film exhibited the maximum water contact angle and a larger zone of inhibition. This film was further used for various characterization and packaging applications.

Characterization of the Bio-Composite

Surface Morphological Study of PLA-SMNC-ZnO NPs Biocomposite

The surface morphology of the nanocomposite films was studied with the help of SEM, focusing on the binding status between ZnO NPs and the PLA-SMNC biocomposite [33]. The samples were examined to understand the biocomposite film's surface comprehensively. Additionally, atomic force microscopy was utilized to analyze the 3D structure and surface roughness of the PLA-SMNC and PLA-SMNC-ZnO NPs film samples, each measuring 2 * 2cm [33, 36].

Structural Analysis of the Bio-Composite

The crystalline or amorphous nature of the PLA and their composites was ascertained by XRD, performed at room temperature using a Cu-Kα source and a generator set at 40 kV and 15mA [33]. As described previously, the functional groups in the PLA-SMNC-ZnO NPs film samples were detected through FTIR analysis.

Mechanical Properties

A testometric machine with grips having a cross-head speed of 50 mm/min and separated at 50 mm was used to assess the mechanical qualities of the film samples. Established procedures were followed to ascertain the tensile strength, elastic modulus, and elongation at break. Tensile strength was computed by dividing the specimen's initial cross-sectional area by the maximum load the film could bear before failing. The linear stress/strain curve's slope was used to calculate the elastic modulus, and the specimen's elongation at break was determined by calculating the percentage change in length between the grips at the point of failure [32, 37, 38].

Thermal Analysis

Thermal gravimetric analysis was performed for the PLA, PLA-SMNC, and PLA-SMNC-ZnO NPs films using a thermogravimetric analyzer. The heating process was conducted in a nitrogen atmosphere, starting from 30 °C and gradually increasing to 600 °C at 10 °C/min [37].

Water Absorption

Samples measuring 2 * 2 cm were submerged in 250 ml of water for 3 days to examine the water absorption capabilities of the PLA, PLA-SMNC, and PLA-SMNC-ZnO NPs films. The change in the weight of the film was measured every 24 h. The composite films were dried at 37 °C before measuring the water absorption percentage. The amount of water absorbed by the film was ascertained by measuring each sample's weight before and after immersion and calculating the difference between the initial and final weights [39].

UV Barrier Analysis

UV−Vis Spectrophotometer analyses the absorbance at 280–400 nm wavelength for PLA, PLA-SMNC, and PLA-SMNC-ZnO NPs films. The samples were cut into regular rectangle shapes (1*4 cm) and placed into the cuvette. The transmittance for both UVA (310–400 nm) and UVB (280–315 nm) were recorded, and the calculation was worked out using the following equations [39]:

$$UVA = \frac{Transmission(315nm + 320nm + \cdots + 400nm)}{18} \quad (2)$$

$$UVB = \frac{Transmission(280nm + 285nm + \cdots + 315nm)}{8} \quad (3)$$

Results and Discussion

Characterization of Synthesized ZnO NPs

UV–Vis Spectroscopy

UV−Vis spectrometry analysis was performed to validate the synthesis of ZnO NPs. UV−Vis spectrometry analysis, ranging from 300 to 400 nm, revealed a distinctive peak at 355 nm, which is the characteristic absorbance peak of ZnO NPs (Fig. 1a). This observation aligns with prior research indicating that the absorbance band of ZnO NPs typically ranges from 315 to 360 nm [40]. Similarly, comparable results were noted during the production of ZnO NPs using zinc nitrate and *B. flabellifer* fruit pulp [29]. Particularly in the UV region, these nanoparticles displayed a distinctive absorbance peak linked to stimulating their surface plasmons (SP). This further emphasizes the influence of nanoparticle size on this phenomenon. Interestingly, the SP resonance bands were observed to shift, either towards the red or blue end, as a result of quantum size effects.

SEM and Zeta Potential Analysis

The surface morphology of the synthesized ZnO NPs was examined using SEM analysis. Fig. 1b captures an image of the ZnO NPs, revealing the arrangement of irregularly shaped particles that are agglomerated and unevenly distributed. The particle size was determined to be approximately 20–30 nm, based on the SEM image analysis using ImageJ software [28]. This aggregation was observed due to the

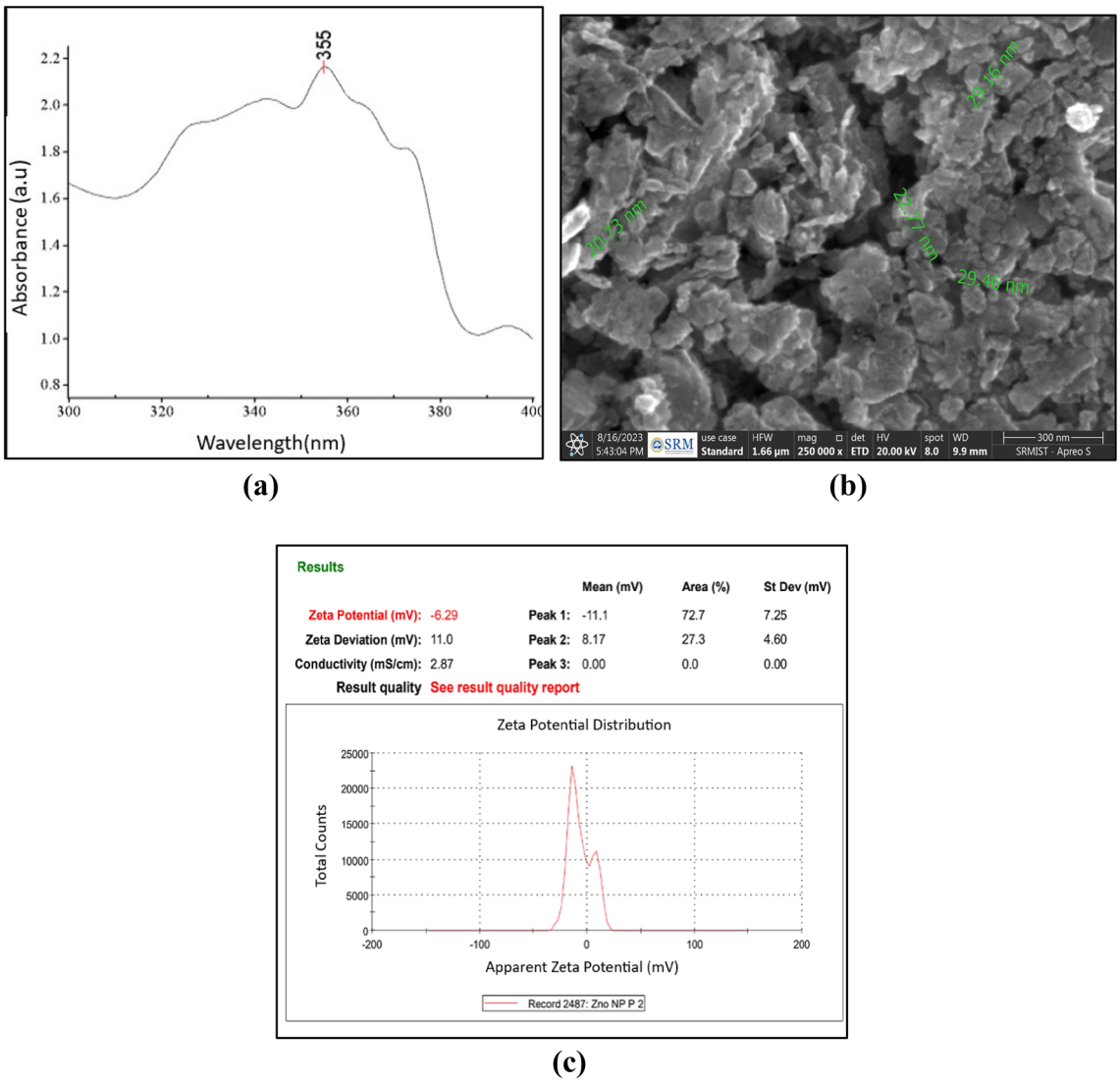

Fig. 1 **a** UV Spectrophotometric analysis of ZnO NPs, **b** SEM analysis of ZnO NPs, **c** Zeta potential of ZnO NPs

interface between the NPs and bio-organic capping particles, aided by hydrogen bonding and electrostatic forces [41]. The zeta potential value of the synthesized ZnO NPs was measured to be − 6.29 mV, indicating the relatively stable nature of the ZnO NPs (Fig. 1c).

FTIR Analysis

The FTIR spectrum depicted in Fig. 2a represents the analysis of the ZnO NPs synthesized by utilizing *B. flabellifer* leaf extract. The main objective of this spectroscopic investigation was to detect the functional groups attributed to the biological molecules accountable for effectively capping and stabilizing the ZnO NPs. The observed peaks within the 3200–3600 cm^{-1} range in the FTIR spectrum correspond to the hydroxyl group stretching of intramolecular hydrogen bonds and the stretching of 'CH' bonds in alkanes [28]. Moreover, the discernible peaks at 1489 were Associated with the absorption band of C–C bonds, while the bands within the 1100–1300 cm^{-1} range indicated the presence of C–N bonds of amines and C–OH groups. Additionally, the vibrations that affect the bond length found between 400 and 750 cm^{-1} indicated the presence of ZnO, specifically equivalent to its stretching mode and a prominent peak at 514 cm^{-1}, corresponding to ZnO [42]. Previous studies have confirmed the existence of a diverse range of compounds within *B. flabellifer*, such as polyphenols, alkaloids, aromatic hydrocarbons, terpenoids, and steroids [29]. As a result, our FTIR analysis revealed the existence of functional groups in the extract's biomolecules, including all the above-listed phytochemicals. These compounds play an important role in the reduction and capping processes of ZnO NPs.

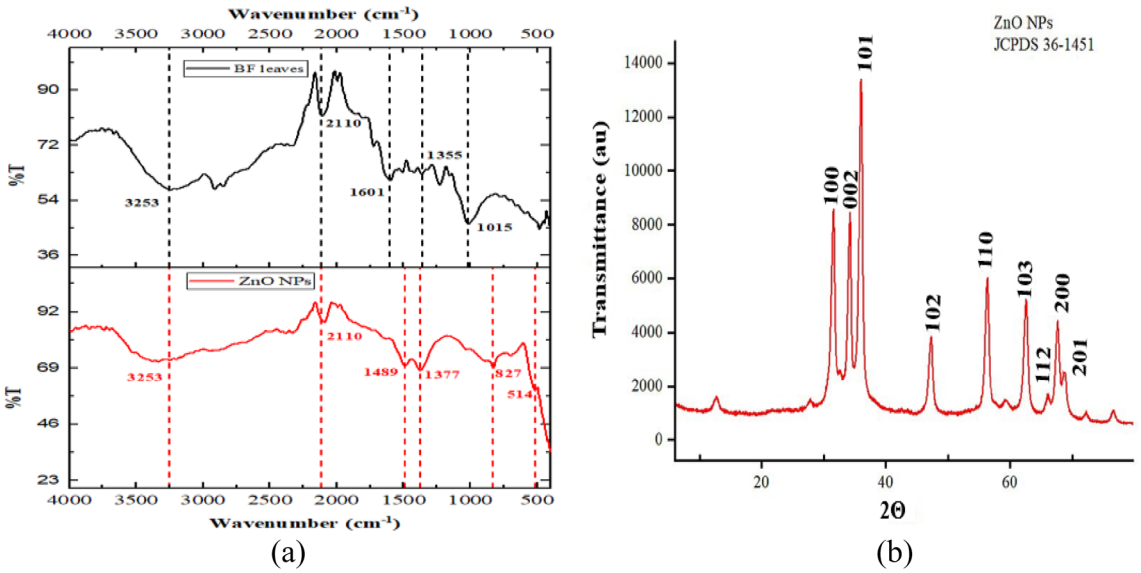

Fig. 2 **a** FTIR analysis of *B. flabellifer* leaves and ZnO NPs, **b** XRD analysis of ZnO NPs

They also prevent the NPs from clumping together in the extract solution. This not only led to the formation of ZnO particles but also highlighted the stabilizing capabilities of the plant extracts, indicating their dual role as both reducing agents and stabilizers.

XRD Analysis

The crystalline structure of the nanoparticles was comprehensively analyzed via XRD. The peaks, observed at specific 2θ values of 47.21°, 56.27°, 62.52°, 67.61°, 68.76°, and 69.02°, were determined to correspond to lattice planes (102), (110), (103), (200), (112), and (201) respectively, as per the JCPDS Card Number (36-1451). By analyzing specific positions of the peaks, such as 31.46°, 34.12°, and 35.94°, the lattice planes (100), (002), and (101) were also identified among others and when compared to the JCPDS card they were found to correspond precisely, confirming the presence of a hexagonal wurtzite crystal structure (Fig. 2b). Significantly, the existence of pristine NPs is indicated by the planes (100), (002), and (101) [24]. Moreover, the size of the NPs was calculated using the Debye–Scherrer equation (Eq. 1). The determined average crystal size of the nanoparticle was 10.67 nm.

Optimization of PLA-SMNC-ZnO NPs Composite

The PLA-SMNC-ZnO NPs blending ratio was optimized by the appearance of the casted film, water contact angle, and antimicrobial properties. The film cast with 1–3% of ZnO NPs were observed to be transparent. Whereas the films with 4–7% were opaque. However, a further increase in the proportion of ZnO NPs resulted in the formation of clusters. Hence, the bio-composite films with 1–7% ZnO NPs were chosen for further optimization.

WCA

WCA is employed to assess the water absorption characteristics of the film. The WCA was found to be increasing as the amount of ZnO NPs increased, which exemplifies the improved film's water-repellent characteristics. An angle exceeding 90° indicates the film's water-repelling nature. Table 1 shows the result of WCA for different compositions of the PLA-SMNC-ZnO NPs composite film. Film compositions with 1 to 3% of ZnO NPs were found to be hydrophilic, as the WCA was measured to be less than 90°. Whereas the films with 4–7% ZnO NPs exhibited WCA of more than 90°, which signifies a hydrophobic nature [43]. The highest water contact angle of 92.5° was measured for the film with 7%

Table 1 Optimization of PLA-SMNC-ZnO NPs ratio based on water contact angle

PLA (wt%)	SMNC (wt% of PLA)	ZnO NPs (wt% of PLA)	WCA(°)
95.5	3.5	1	48
94.5	3.5	2	51.5
93.5	3.5	3	75.5
92.5	3.5	4	80.5
91.5	3.5	5	83
90.5	3.5	6	86.4
89.5	3.5	7	92.5

ZnO NPs. The findings were similar to the results reported for PLA-ZnO NPs composite [44].

Antimicrobial Assay

The antimicrobial activity of the PLA-SMNC-ZnO NPs (3–7%) was evaluated against both the Gram(− ve) bacteria *E. coli* and Gram(+ ve) bacteria *S. aureus*. The zone of inhibition was observed by measuring the dimensions of the clear areas encircling the biocomposite film (Fig. 3a and b). The film with 3% Zno NPs did not show any significant antibacterial activity. Figure 4 shows the measured zone of inhibition values of the PLA-SMNC-ZnO NPs films for *E. coli* and *S. aureus*. This study observed that the inhibitory effects of the film on both microbes were enhanced as the concentration of ZnO NPs increased from 4 to 7%. Specifically, the inhibition zone for *E. coli* showed a significant increase from 25 to 32 mm, while for *S. aureus*, it increased from 21 to 35 mm. These results are in accordance with a previous study conducted by Ghozali et al. [35], where the highest concentration of ZnO additives also leads to the widest clear zone. This suggests that the direct interaction between the metal oxide and the bacterial cell wall may play a crucial role in the observed antibacterial effects as it leads to damage to the cell. Additionally, the reactive sites of the metal oxide likely facilitate the antibacterial activities observed in this study [45].

The antibacterial mechanism of PLA-SMNC-ZnO NPs films on the studied bacteria is mainly attributed to the release of Zn^{2+} ions and the generation of reactive oxygen species (ROS). The ROS generated include hydroxyl radicals (·OH) and ions (OH^-), hydrogen peroxide (H_2O_2), superoxide anions (O_2^-) and hydroperoxyl radicals (HOO·). Nanoparticles gather on the surface of bacterial cell membranes and destroy them. Furthermore, the cytotoxic action of ZnO nanomaterials is believed to be caused by physical electrostatic interactions between surfaces of bacterial cells with different charges, mechanical damage to cell envelopes, particle penetration, internalization, and accumulation within the cells. These factors are

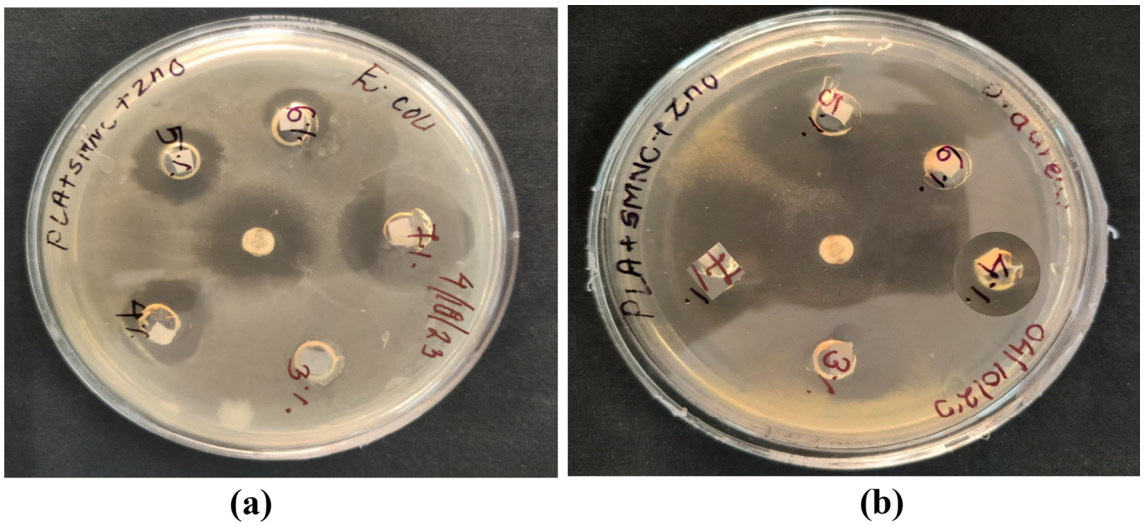

Fig. 3 Antimicrobial assay of PLA-SMNC-ZnO NPs against **a** *E. coli*, and **b** *S. aureus*

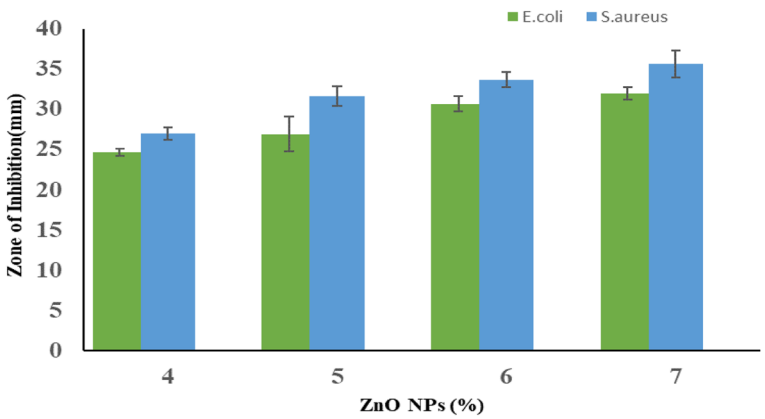

Fig. 4 Zone of inhibition of PLA-SMNC-ZnO NPs films for *E. coli* and *S. aureus*

all proposed to contribute to the destruction of bacterial cells by ZnO nanomaterials [46, 47].

The incorporation of ZnO NPs into the PLA-SMNC film has also been shown to enhance surface roughness, a crucial factor in strengthening the antimicrobial properties of ZnO NPs in the film. This increase in roughness results in a greater effective surface area compared to the previously geometrically flat region. This expansion is expected to lead to a higher production of active species, such as ions and ROS, which are responsible for the antimicrobial effects. Additionally, the added roughness provides a larger surface area for bacterial attachment. This aligns with recent research by Valireini et al. [48], which demonstrated that rougher surfaces promote increased bacterial adhesion through physical interactions with bacterial cell walls. With the augmentation in adhesion between materials and bacteria, a nuanced structural metamorphosis ensues. This transformative process fortifies the defence against microbes, encompassing heightened abrasive impacts and the conveyance of active agents from the material's surface to bacterial cells.

Characterization of the PLA-SMNC-ZnO NPs Composite

Surface Morphological Study

The surface level morphology of the PLA and its composite films were investigated using SEM (Fig. 5). Smooth and flat surface of the neat PLA was free of noticeable cracks, voids, or air pockets (Fig. 5a). Significant changes in the microstructures of the film were detected after introducing 3.5 wt% SMNC into the PLA matrix. The PLA-SMNC film, in particular, showed the development of pores inside the matrix (Fig. 5b), with diameters ranging from 3 to 8 nm. Although porous films are frequently used in biomedical applications, the PLA-SMNC composite alone may not be ideal for any application due to its porosity structure, which

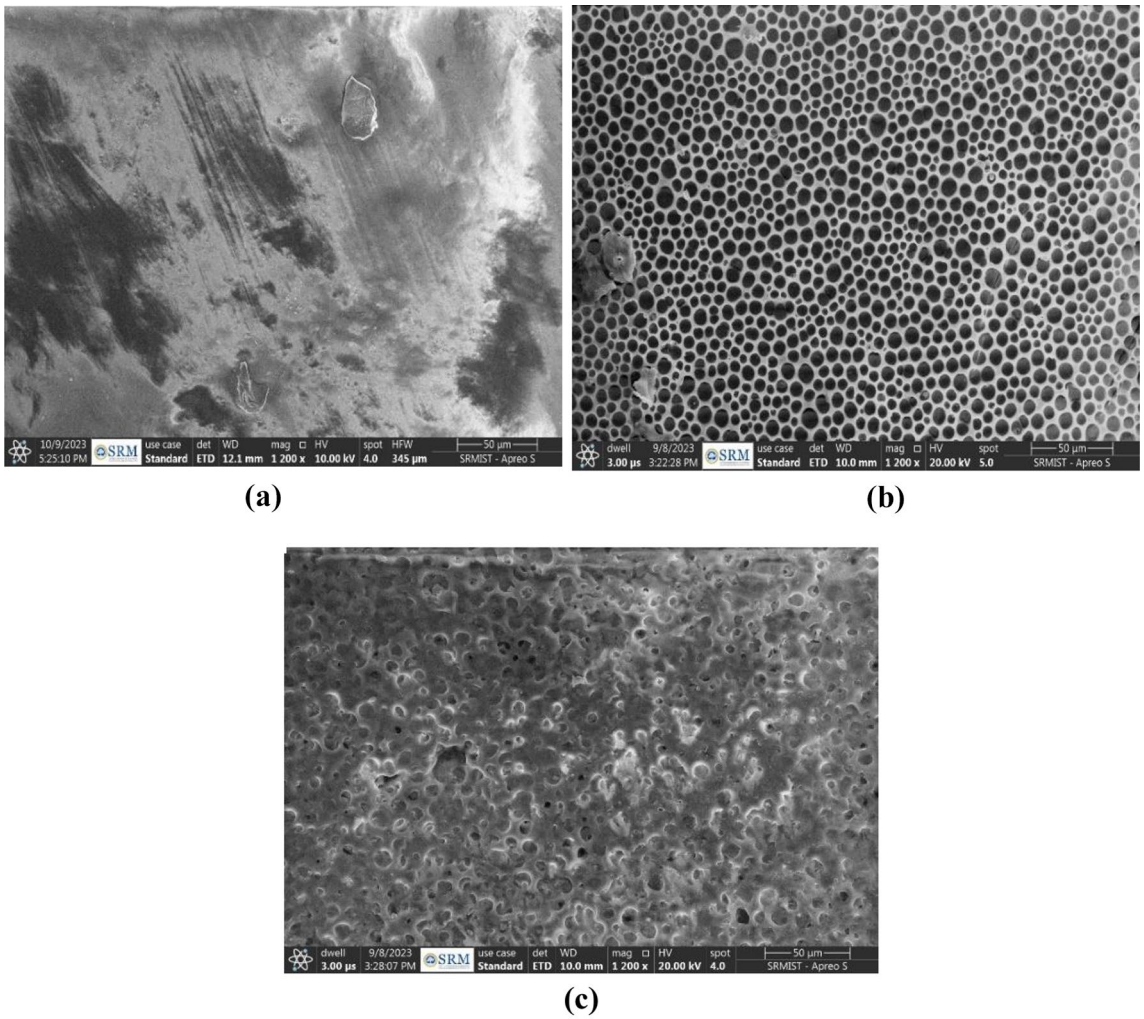

Fig. 5 SEM analysis of **a** PLA, **b** PLA-SMNC, and **c** PLA-SMNC-ZnO NPs films

may compromise the film's migratory qualities [49]. As ZnO NPs were further integrated into the matrix, the SEM analysis exposed a seamless distribution of ZnO NPs throughout the PLA-SMNC matrix (Fig. 5c). The addition of ZnO NPs notably decreased the film's porosity due to the favorable integration of ZnO NPs with both PLA and SMNC.

AFM analysis, a highly advanced imaging technique for scanning and measuring minuscule features on surfaces, was adopted to explore the surface morphology and roughness of PLA, PLA-SMNC, and PLA-SMNC-ZnO NPs films (Fig. 6). Upon performing AFM analysis on the PLA film, it was evident that the surface was sleek, potentially raising concerns for its use in packaging (Fig. 6a). However, the PLA-SMNC film had discernible pores. Due to these pores, this composite was still unsuitable for many applications (Fig. 6b). Conversely, the AFM image of the PLA-SMNC-ZnO NPs film showed an absence of pores and small peak-like protrusions due to the clustering of ZnO NPs within the film (Fig. 6c). Additionally, there was an increase in surface roughness compared to the original PLA film. Surfaces with higher levels of roughness can enhance their hydrophobic properties. This is because of the air trapped by hydrophobic surfaces, which becomes even more effective with increased roughness, according to Wan et al. [50]. As a result, it can be concluded that incorporating ZnO NPs into the PLA-SMNC matrix has led to a noticeable improvement in hydrophobicity and a reduction in pore formation in the film, making it

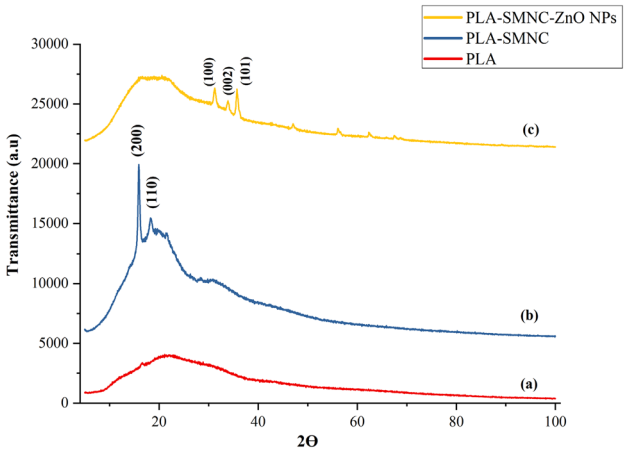

Fig. 7 XRD analysis of **a** PLA, **b** PLA-SMNC, and **c** PLA-SMNC-ZnO NPs films

suitable for many applications. Similar research by Nonato et al. [51] has also emphasized the beneficial impact of ZnO NPs on improving the surface roughness of PLA films.

Structural Analysis

The crystallographic characteristics of PLA and different PLA biocomposites were investigated using XRD and depicted in Fig. 7. While the neat PLA exhibited largely

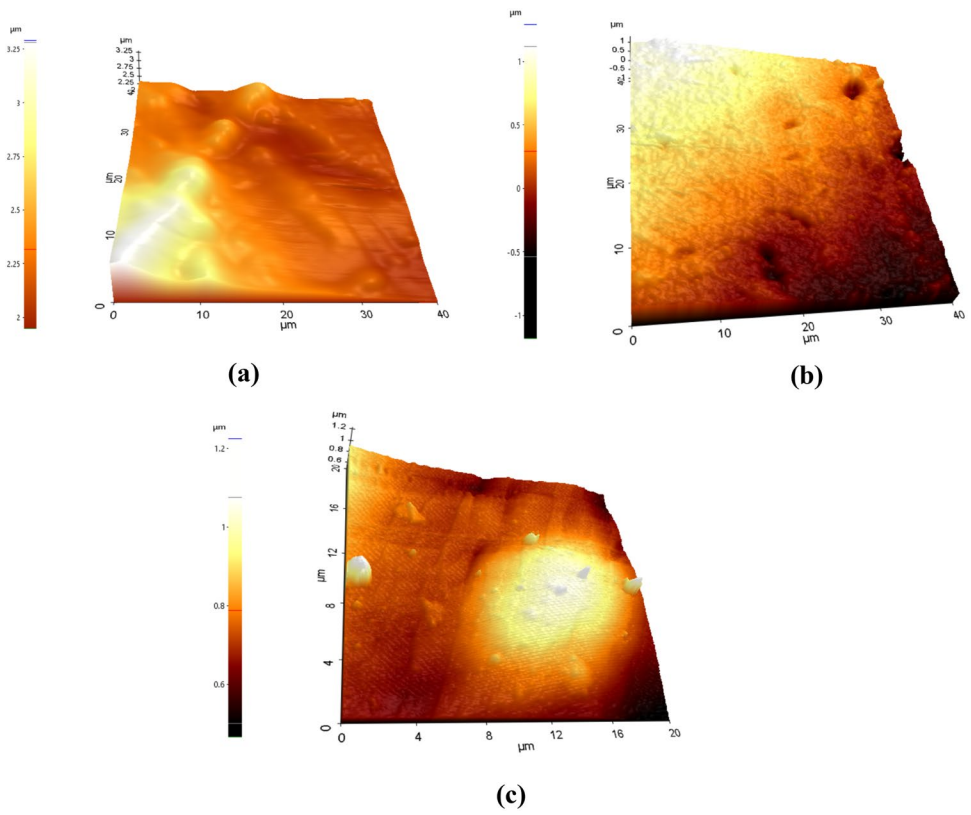

Fig. 6 AFM analysis of **a** PLA, **b** PLA-SMNC, and **c** PLA-SMNC-ZnO NPs films

amorphous structures with no discernible crystallization, the PLA-SMNC composite exhibited prominent peaks at approximately 15.90° and 18.27° of 2θ, indicating the presence of (200) and (110) planes, respectively. These findings suggest that PLA follows an orthorhombic structure with three unequal axes at right angles to each other within its crystalline system [52]. After incorporating ZnO NPs, the intensities of the two peaks associated with PLA's crystallinity decreased, but this did not diminish the ZnO NPs' ability to promote PLA crystallization. Moreover, distinct diffraction peaks at 31.31°, 33.92°, and 35.68° were identified in the XRD patterns of the PLA-SMNC-ZnO NPs composite films. These peaks corresponded to the (100), (002), and (101) crystal planes of ZnO, respectively [53].

From the FTIR graph, the presence of various functional groups was explored (Fig. 8). The vibration of the hydroxyl bonds in the PLA molecules was thought to be the cause of the unique band at 3653 cm^{-1} that was seen in the pure PLA film. It was determined that the stretching of the -CH_3 group was responsible for another peak at 2935 cm^{-1}. Notably, the sharp peak at 1739 cm^{-1} corresponds to the vibrations that affect the bond length of carbonyl bonds in the ester groups of the PLA structure. Furthermore, the peaks at 1444 cm^{-1} and 1352 cm^{-1} were suggestive of symmetrical and asymmetrical bend vibrations of C-H bonds, revealing more about the film's molecular structure. The strength of the carbonyl group peak was reduced in the PLA-SMNC film. This is believed to be due to hydrogen bond formation between the PLA matrix's carbonyl groups and the SMNC's hydroxyl groups. Interestingly, the PLA-SMNC composite exhibited identical peaks to the pure PLA spectra but at differing intensities. This implies that the presence of SMNC affects the features of these peaks. By including ZnO NPs, the carbonyl group stretching vibration peak was effectively moved to a lower wavelength, demonstrating the possibility of intermolecular interactions between PLA, SMNC, and ZnO NPs. Additionally, the emergence of a novel band at 421 cm^{-1} substantiated the successful inclusion and integration of ZnO NPs into the PLA-SMNC composite, reinforcing the incorporation procedure [28, 30, 42].

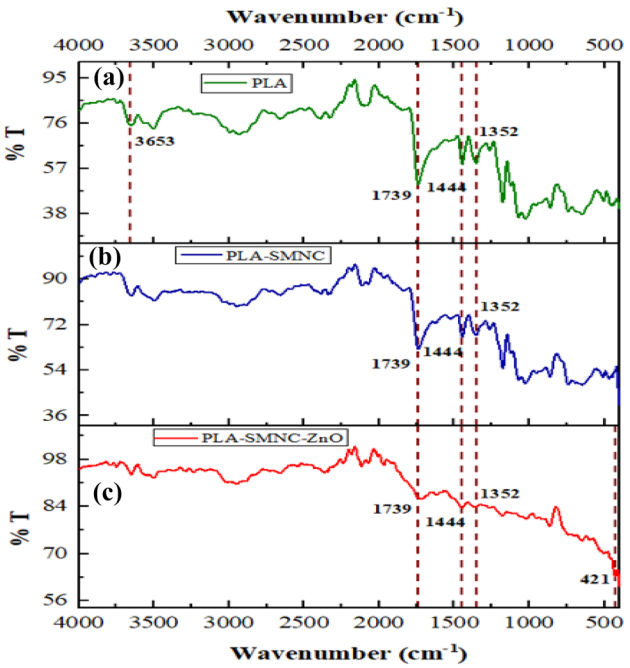

Fig. 8 FTIR analysis of **a** PLA, **b** PLA-SMNC, and **c** PLA-SMNC-ZnO NPs films

Mechanical Properties

The mechanical characteristics of PLA biocomposite films were meticulously assessed in Universal Testing Systems for tensile, compression, and flexure testing equipped with a 0.5 kN frame capacity. The tensile properties were thoroughly evaluated by subjecting samples with a width of 20 and 70 mm long to a cross-head velocity of 2 mm/min. Table 2 displays the varying thicknesses of PLA-based biocomposite films. Initially, the PLA film had a thickness of 0.220 mm, but with the addition of SMNC, the thickness was reduced to 0.120 mm. It is worth noting that the PLA-SMNC-ZnO NPs biocomposite showed a significant decrease in thickness compared to the neat PLA film. However, the thickness of PLA-SMNC-ZnO NPs was more than that of the PLA-SMNC composite film. Table 1 provides a comprehensive analysis of several mechanical parameters, including tensile strength (TS), Young's modulus (EM), ultimate force, break distance, and total elongation break (EB) of different PLA biocomposite films and the neat PLA film. The TS evaluates the utmost stress the film can endure before fracturing. For the pure PLA film, this was found to be 12.1 MPa. Nevertheless, the inclusion of SMNC led to a reduction in TS, presumably owing to insufficient interfacial bonding between the SMNC and the PLA matrix. Conversely, the addition of 7 wt% of ZnO NPs to the PLA-SMNC composite, resulted in a significant increase in the TS of 14.87% over the plain

Table 2 Mechanical property analysis: (a)PLA, (b)PLA-SMNC, (c) PLA-SMNC-ZnO NPs films

	PLA	PLA-SMNC	PLA-SMNC-ZnO NPs
Tensile strength (MPa)	12.1	10.1	13.9
Young's modulus (GPa)	0.00307	0.00303	0.00689
Ultimate force (N)	46.8	19.8	40.4
Break distance (mm)	26.9	17.9	6.60
Total elongation break (%)	67.3	44.8	16.5
Thickness (mm)	0.22	0.12	0.16

PLA film and 32.62% over the PLA-SMNC film. This is likely due to the effective dispersion of ZnO NPs in the PLA matrix, promoting the establishment of robust intermolecular hydrogen bonds between the constituents of the film. Alterations in tensile strength and elongation values might be attributed to the creation of hydrogen bonds between the (−OH) groups in SMNC and the (O_2) atoms within the ZnO-NPs [54].

However, the flexibility of the PLA film was negatively impacted by the addition of SMNC and ZnO, as evidenced by a decrease in its overall EB. The EB of the PLA- SMNC-ZnO NPs composite film notably decreased by 75.48% compared to the neat PLA film and 63.17% compared to the PLA-SMNC film, signifying reduced flexibility in the composite film. This phenomenon was ascribed to the restrictive influence of stiff SMNC and ZnO NPs on the motion of PLA molecular structures, consequently limiting the EB. The decreased EB in the PLA-SMNC-ZnO NPs film is likely due to the clustering and uneven distribution of ZnO-NPs, and the recrystallization of the ZnO-NPs in the polymer matrix [54]. Similarly, findings by Yu et al. [30] align with this trend, confirming the enhancement of various mechanical properties while negatively impacting a few through the addition of ZnO NPs to both neat PLA and PLA-SMNC composite.

Thermal Properties

Thermal assessments of PLA, PLA-SMNC, and PLA-SMNC-ZnO NP films were conducted using TGA and DTG techniques, as shown in Fig. 9a and b respectively. The analysis indicated significant disparities in the thermal characteristics among the various film types. TGA outcomes unveiled a two-stage degradation mechanism for pure PLA and its composite forms. For PLA, the first stage of degradation is initiated at 84 °C, which resulted in an almost 8% reduction in weight and complete degradation observed at 384. During the first degradation stage of PLA-SMNC, the weight decreased by 7% at 170 °C, with a complete loss occurring at 381 °C. This weight loss might be ascribed to moisture evaporation inside the coatings. Similarly, in the PLA-SMNC-ZnO NPs composite, there was a 4% reduction in weight at 147 °C during the initial degradation stage, and complete weight loss was attained at 320 °C. However, the inclusion of ZnO NPs in the nanocomposite films noticeably decreased their thermal resistance compared to the pure PLA film. This may be due to the degrading effect of ZnO NPs on PLA at higher temperatures. These findings corroborated with the conclusions of previous studies by Suryanegara et al. [55] and Shankar et al. [56], which also reported a decrease in PLA's thermal stability with the incorporation of ZnO NPs. Murariu and colleagues proposed a theory suggesting that zinc compounds initiate a chemical process where transesterification reactions between the molecules are catalyzed, leading to the creation of PLA with reduced molecular weight. Additionally, depolymerization occurs, resulting in the formation of lactic acid at higher temperatures [57].

Water Absorption

For evaluating the water absorption properties of PLA biocomposite films, a comprehensive water absorption test was conducted, and the findings are graphically displayed

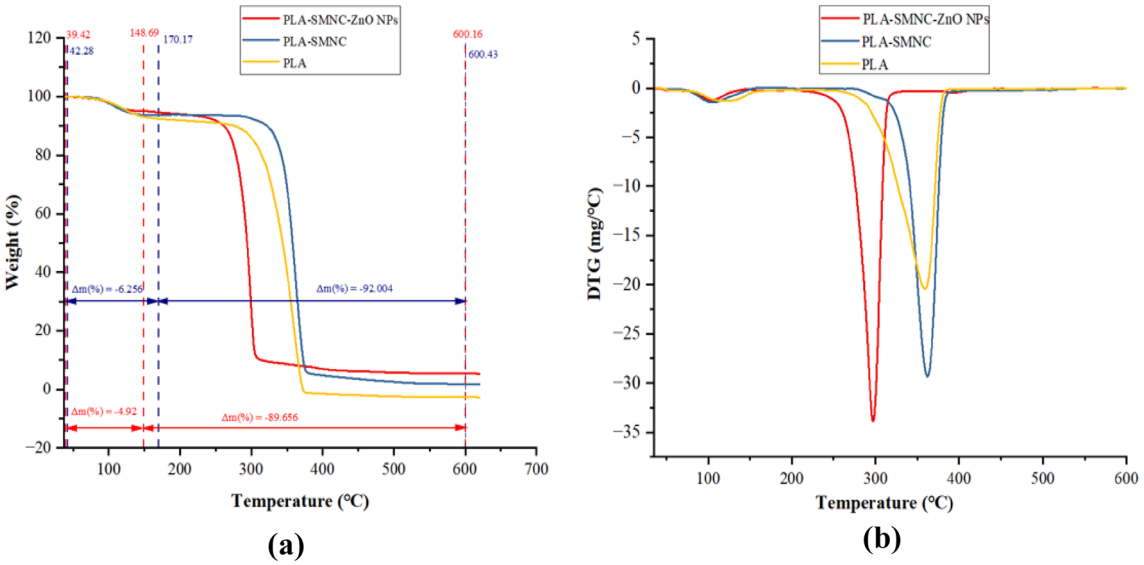

Fig. 9 **a** TGA anlaysis of PLA, PLA-SMC, and PLA-SMNC-ZnO NPs films, and **b** DTG analysis of PLA, PLA-SMNC, and PLA-SMNC-ZnO NPs films

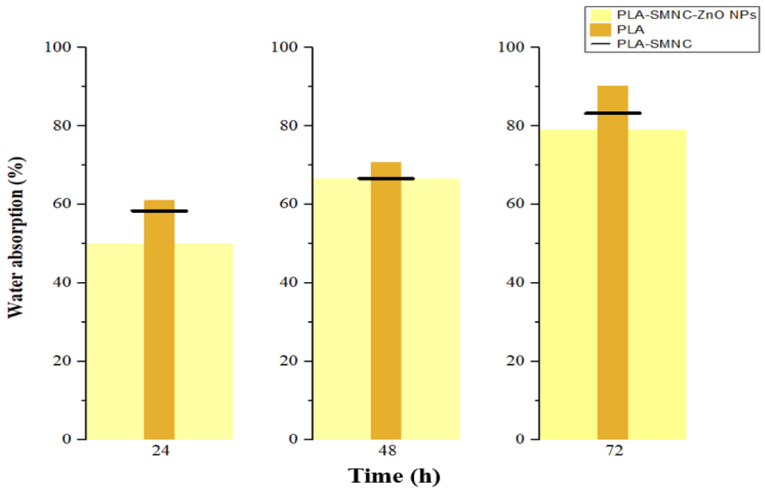

Fig. 10 Water absorption analysis for PLA, PLA-SMNC, and PLA-SMNC-ZnO NPs films

in Fig. 10. Water absorption in films is affected by several parameters, including exposed surface area, fluid temperature, diffusivity, fibre content, the span of exposure, and film orientation. In this study, a 2 * 2 cm film sample was submerged in water for 3 days, and the percentage of weight loss was used as an indicator for water absorption. The findings unmistakably demonstrate that the pure PLA film exhibits a significantly greater water absorption rate in comparison to both the PLA-SMNC and PLA-SMNC-ZnO NPs films, underscoring the enhanced water resistance of the latter. Notably, there was a substantial difference of approx. 10.97% in water absorption between the PLA and PLA-SMNC-ZnO NPs films. After 24 h of immersion, an 8.3% difference was observed between the PLA-SMNC and PLA-SMNC-ZnO NPs films. Even after 72 h, this trend persisted, showcasing the sustained water-resistant capabilities of the PLA-SMNC-ZnO NPs film. The findings strongly indicate that the PLA-SMNC-ZnO NPs film is highly suitable for packaging usage, as it outperforms both PLA and PLA-SMNC films regarding water absorption. Moreover, numerous studies have highlighted the significant advantage of using this film in packaging food products, as it effectively prevents spoilage owing to its lower water absorption properties. The observed results were found to be analogous to the previous studies by Drelich et al. [58] and Rahman et al. [59], both concluded that neat PLA has a greater susceptibility to water absorption than the PLA-SMNC composite and that PLA-ZnO composites possess superior barrier properties compared to neat PLA. The findings further emphasize the improved barrier properties of the PLA-SMNC film due to the integration of ZnO NPs. The water absorption of PLA-SMNC-ZnO NPs films is lower than PLA-SMNC films due to the hydrophobic nature of ZnO NPs and the strong interfacial adhesion between the ZnO NPs and the SMNC matrix. The hydrophobicity of ZnO NPs reduces the water uptake of the PLA-SMNC-ZnO NPs films, which in turn improves their water resistance [48].

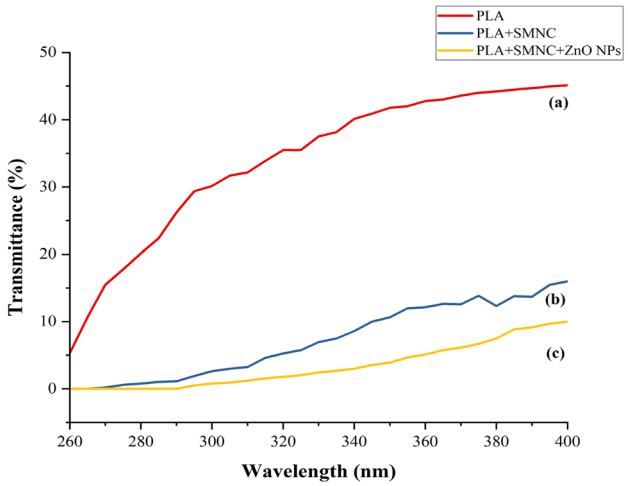

Fig. 11 UV stability test for **a** PLA, **b** PLA-SMNC, and **c** PLA-SMNC-ZnO NPs films

UV Barrier Analysis

UV rays, spanning a range of 100 to 400 nm, comprise UVA, UVB, and UVC types. A protective phenomenon occurs upon encountering the ozone layer, preventing UVC rays from reaching the Earth's surface. Despite this shielding, UVA and UVB rays successfully penetrate the Earth's atmosphere. UVA rays possess wavelengths within 315 to 400 nm, while UVB rays range from 280 to 315 nm. When these rays interact with UV-sensitive materials and biopolymers, they can cause material degradation and initiate chemical processes [37]. To better understand this phenomenon,

an investigation was conducted to determine the transmission percentage of UV rays through PLA-SMNC and PLA-SMNC-ZnO NPs films.

The PLA film exhibited a UV ray transmission of nearly 45%, compared to only about 16% for the PLA-SMNC film and approximately 10% for the PLA-SMNC-ZnO NPs film, as illustrated in Fig. 11. This indicates a significant 35% decrease in UV ray transmission when comparing the PLA-SMNC-ZnO NPs film to the standard PLA film. Additionally, there was a slight reduction of 6% when comparing the PLA-SMNC and PLA-SMNC-ZnO NPs films. It is noteworthy that none of the films showed any transmission in the UVC range of 100–280 nm. In terms of UVA rays, the PLA film had a transmission of 41.232%, while the PLA-SMNC film had a lower transmission of 10.768%, and the PLA-SMNC-ZnO NPs film showed the lowest transmission of 5.247%. By adding 7% ZnO NPs to the PLA matrix, a notable decrease from 41.232 to 5.247%, underscoring the efficacy of SMNC in bolstering the UV-blocking capabilities of PLA.

The observed decrease in UV transmission of PLA-SMNC-ZnO NPs films is due to the synergistic effect of SMNC and ZnO NPs. SMNC is a biodegradable and renewable material that is used as a matrix in the production of biocomposite films. The precise composition of nanostructures plays a vital role in manipulating the energy gap of materials, ultimately leading to targeted absorption of UV bands while maintaining low absorbance in the visible range. As previously investigated, the energy gap determines the range of light wavelengths a material can capture. Inorganic materials such as ZnO are renowned for their wide energy gaps and offer excellent potential in designing UV-protective coatings [60]. Because of this, it is known for its UV-blocking properties. Whereas SMNC has been shown to have UV-absorbing properties that can reduce the transmission of UV radiation. The incorporation of ZnO NPs into the SMNC matrix leads to the formation of a network structure that enhances the interfacial adhesion between the ZnO NPs and the SMNC matrix [61–63]. Previous studies, such as those conducted by Shankar et al. [53], have also illustrated the UV light-blocking properties of ZnO NPs when integrated into a PLA matrix. In conclusion, including SMNC and ZnO NPs in the PLA matrix enhances its ability to withstand UV radiation, thereby improving its overall durability. Evidently, the significant changes in the transmission percentage were due to the integration of SMNC and ZnO NPs obtained from *B. flabellifer* leaves into the PLA matrix.

Conclusion

The study on PLA-based composites, enriched with SMNC and ZnO NPs derived from *B. flabellifer* leaves, has unveiled significant advancements that render these composite materials highly versatile for a multitude of applications. Inextricably tied to human necessities throughout history, the *B. flabellifer* tree bears both economic and social significance. Its leaves, known for their high cellulose content and natural fibers, lend exceptional mechanical strength and UV stability to materials. Additionally, ZnO NPs derived from the same source alleviate compatibility issues with PLA in the PLA-SMNC-ZnO NPs composite. Furthermore, by incorporating cellulose and ZnO NPs obtained from repurposed waste tree leaves, the approach exemplifies sustainable resource utilization without necessitating dedicated tree harvesting. This unique amalgamation of utilizing discarded materials and unconventional sources for cellulose and ZnO NPs underscores the cost-effectiveness and eco-friendliness inherent in the composition of PLA-SMNC-ZnO NPs films. The successful integration of ZnO NPs within the PLA-SMNC matrix has notably improved the film's robustness, making it well-suited for various industrial uses. Notably, the PLA-SMNC-ZnO NPs composite exhibited enhanced mechanical properties, including increased TS and EM compared to the pure PLA and PLA-SMNC films. This improvement can be attributed to the effective integration of ZnO NPs, strengthening intermolecular bonds and reinforcing structural stability. Additionally, the films demonstrated reduced water absorption and increased hydrophobicity, showcasing their potential for moisture-resistant and barrier applications. Moreover, the antibacterial efficacy against *E. coli* and *S. aureus* bacteria makes these films particularly promising for safeguarding packaged goods from potential microbial threats. Furthermore, the significant enhancement in UV stability broadens their practical applications, particularly in settings where prolonged exposure to sunlight is expected. Furthermore, conducting thorough evaluations of these biocomposite films' biodegradability and environmental impact in different scenarios could yield vital insights for their widespread use in various industries, such as food packaging, medicine, and sustainable consumer goods.

Acknowledgements The authors sincerely thank the Department of Biotechnology, SRM Institute of Science and Technology, for providing research and analytical facilities. The authors express their gratitude to Mr. Kumaran Panjanathan for generously supplying the leaves.

Author Contributions PG: Methodology, investigation, formal analysis of data, validation, and preparation of original draft; PMR: Methodology, investigation, formal analysis of data, and preparation of original draft; SS: Methodology, investigation, formal analysis of data, and preparation of original draft; AVS: Methodology, investigation, formal analysis of data, and preparation of original draft; PR: Conceptualization, supervision, Writing—Review and editing.

Funding Not applicable.

Declarations

Competing Interests The authors declare no competing interests.

Ethical Approval Not applicable.

Consent to Publish All authors have agreed to publish the paper.

References

1. Turan K (2015) Green materials and applications. Period Eng Nat Sci 3(2):1–7
2. Flórez M, Cazón P, Vázquez M (2023) Selected biopolymers' Processing and their applications. Rev Polym J 15(3):641. https://doi.org/10.3390/polym15030641
3. Vieira MGA, da Silva MA, dos Santos LO, Beppu MM (2011) Natural-based plasticizers and biopolymer films: a review. Eur Polym J 47(3):254–263. https://doi.org/10.1016/j.eurpolymj.2010.12.011
4. El-latief RAEA (2018) Asphalt Modified with Biomaterials as Eco-Friendly and Sustainable Modifiers. In Modified Asphalt. InTech. https://doi.org/10.5772/intechopen.76832
5. Ncube LK, Ude AU, Ogunmuyiwa EN, Zulkifli R, Beas IN (2020) Environmental impact of Food Packaging materials: a review of Contemporary Development from Conventional Plastics to Polylactic. Acid Based Mater Mater 13(21):4994. https://doi.org/10.3390/ma13214994
6. Pamuk G (2016) Natural fibres Reinforced Green composites. Tekstilec 59(3):237–243. https://doi.org/10.14502/Tekstilec2016.59.237-243
7. Cavallo E, He X, Luzi F, Dominici F, Cerrutti P, Bernal C, Foresti ml, Torre L, Puglia D (2020) UV protective, antioxidant, Antibacterial and Compostable Polylactic Acid composites containing pristine and chemically modified lignin nanoparticles. Molecules 26(1):126. https://doi.org/10.3390/molecules26010126
8. Sun Z, Zhang L, Liang D, Xiao W, Lin J (2017) Mechanical and thermal properties of PLA biocomposites Reinforced by Coir fibers. Int J Polym Sci 2017:1–8. https://doi.org/10.1155/2017/2178329
9. Dai L, Li R, Liang Y, Liu Y, Zhang W, Shi S (2022) Development of Pomegranate Peel Extract and Nano ZnO Co-reinforced Polylactic Acid Film for active food packaging. Membr J 12(11):1108. https://doi.org/10.3390/membranes12111108
10. Eom Y, Choi B, Park S (2019) A study on Mechanical and Thermal properties of PLA/PEO blends. J Polym Environ 27(2):256–262. https://doi.org/10.1007/s10924-018-1344-y
11. Piekarska K, Sowinski P, Piorkowska E, Haque MM-U, Pracella M (2016) Structure and properties of hybrid PLA nanocomposites with inorganic nanofillers and cellulose fibers. Compos A: Appl 82:34–41. https://doi.org/10.1016/j.compositesa.2015.11.019
12. Sun J, Shen J, Chen S, Cooper M, Fu H, Wu D, Yang Z (2018) Nanofiller Reinforced Biodegradable PLA/PHA composites: current Status and Future trends. Polym J 10(5):505. https://doi.org/10.3390/polym10050505
13. Wang Y, Liu S, Wang Q, Ji X, Yang G, Chen J, Fatehi P (2021) Strong, ductile and biodegradable polylactic acid/lignin-containing cellulose nanofibril composites with improved thermal and barrier properties. Ind Crops Prod 171:113898. https://doi.org/10.1016/j.indcrop.2021.113898
14. Athinarayanan J, Alshatwi AA, Subbarayan Periasamy V (2020) Biocompatibility analysis of Borassus flabellifer biomass-derived nanofibrillated cellulose. Carbohydr Polym 235:115961. https://doi.org/10.1016/j.carbpol.2020.115961
15. Shanmugam D, Thiruchitrambalam M (2013) Static and dynamic mechanical properties of alkali treated unidirectional continuous Palmyra Palm Leaf Stalk Fiber/jute fiber reinforced hybrid polyester composites. Mater Des 50:533–542. https://doi.org/10.1016/j.matdes.2013.03.048
16. Ghasemlou M, Daver F, Ivanova EP, Habibi Y, Adhikari B (2021) Surface modifications of nanocellulose: from synthesis to high-performance nanocomposites. Prog Polym Sci 119:101418. https://doi.org/10.1016/j.progpolymsci.2021.101418
17. Coma V, Freire CSR, Silvestre AJD (2015) Recent advances on the development of Antibacterial Polysaccharide-based materials. Polysaccharides. Springer International Publishing, Cham, pp 1751–1803. doi: https://doi.org/10.1007/978-3-319-16298-0_12
18. Nemeş NS, Ardean C, Davidescu CM, Negrea A, Ciopec M, Duţeanu N, Negrea P, Paul C, Duda-Seiman D, Muntean D (2022) Antimicrobial activity of Cellulose based materials. Polymers 14(4):735. https://doi.org/10.3390/polym14040735
19. Hassaan MA, Nemr E, A., Ragab S (2021) Green Synthesis and Application of Metal and Metal Oxide nanoparticles. Handbook of nanomaterials and nanocomposites for Energy and Environmental Applications. Springer International Publishing, Cham, pp 831–857. doi: https://doi.org/10.1007/978-3-030-36268-3_125
20. Khan S, Katsumata K, Rodríguez-González V, Terashima C, Fujishima A (2021) Gas-phase synthesis for Mass production of TiO2 nanoparticles for environmental applications. Handbook of nanomaterials and nanocomposites for Energy and Environmental Applications. Springer International Publishing, Cham, pp 953–973. doi: https://doi.org/10.1007/978-3-030-36268-3_10
21. Kumar SS, Venkateswarlu P, Rao VR, Rao GN (2013) Synthesis, characterization and optical properties of zinc oxide nanoparticles. Int Nano Lett 3(1):30. https://doi.org/10.1186/2228-5326-3-30
22. Espitia PJP, Soares N, de FF, Coimbra dos R. JS, de Andrade NJ, Cruz RS, Medeiros EAA (2012) Zinc oxide nanoparticles: synthesis, antimicrobial activity and food packaging applications. Food Bioproc Tech 5(5):1447–1464. https://doi.org/10.1007/s11947-012-0797-6
23. Faisal S, Jan H, Shah SA, Shah S, Khan A, Akbar MT, Rizwan M, Jan F, Wajidullah, Akhtar N, Khattak A, Syed S (2021) Green synthesis of zinc oxide (ZnO) nanoparticles using aqueous fruit extracts of *Myristica fragrans*: their characterizations and Biological and Environmental Applications. ACS Omega 6(14):9709–9722. https://doi.org/10.1021/acsomega.1c00310
24. Rajeshkumar S, Kumar SV, Ramaiah A, Agarwal H, Lakshmi T, Roopan SM (2018) Biosynthesis of zinc oxide nanoparticles usingMangifera indica leaves and evaluation of their antioxidant and cytotoxic properties in lung cancer (A549) cells. Enzyme Microb Technol 117:91–95. https://doi.org/10.1016/j.enzmictec.2018.06.009
25. Eswari KM, Asaithambi S, Karuppaiah M, Sakthivel P, Balaji V, Ponelakkia DK, Yuvakkumar R, Kumar P, Vijayaprabhu N,G, R (2022) Green synthesis of ZnO nanoparticles using Abutilon Indicum and Tectona Grandis leaf extracts for evaluation of antidiabetic, anti-inflammatory and in-vitro cytotoxicity activities. Ceram Int 48(22):33624–33634. https://doi.org/10.1016/j.ceramint.2022.07.308
26. Umavathi S, Subash M, Gopinath K, Alarifi S, Nicoletti M, Govindarajan M (2021) Facile synthesis and characterization of ZnO nanoparticles using Abutilon indicum leaf extract: an eco-friendly nano-drug on human microbial pathogens. J Drug Deliv Sci Technol 66:102917. https://doi.org/10.1016/j.jddst.2021.102917
27. Ramesh P, Saravanan K, Manogar P, Johnson J, Vinoth E, Mayakannan M (2021) Green synthesis and characterization of biocompatible zinc oxide nanoparticles and evaluation of its antibacterial

potential. Sens Bio-Sens Res 31:100399. https://doi.org/10.1016/j.sbsr.2021.100399
28. Rahman F, Majed Patwary MA, Bakar Siddique MA, Bashar MS, Haque MA, Akter B, Rashid R, Haque MA, Uddin R (2022) Green synthesis of zinc oxide nanoparticles using Cocos nucifera leaf extract: characterization, antimicrobial, antioxidant and photocatalytic activity. R Soc Open Sci. https://doi.org/10.1098/rsos.220858
29. Vimala K, Sundarraj S, Paulpandi M, Vengatesan S, Kannan S (2014) Green synthesized doxorubicin loaded zinc oxide nanoparticles regulate the Bax and Bcl-2 expression in breast and colon carcinoma. Process Biochem 49(1):160–172. https://doi.org/10.1016/j.procbio.2013.10.007
30. Arun R, Shruthy R, Preetha R, Sreejit V (2022) Biodegradable nanocomposite reinforced with cellulose nanofiber from coconut industry waste for replacing synthetic plastic food packaging. Chemosphere 291:132786
31. Wei L, Agarwal UP, Hirth KC, Matuana LM, Sabo RC, Stark NM (2017) Chemical modification of nanocellulose with canola oil fatty acid methyl ester. Carbohydr Polym 169:108–116
32. Yu F, Fei X, He Y, Li H (2021) Poly (lactic acid)-based composite film reinforced with acetylated cellulose nanocrystals and ZnO nanoparticles for active food packaging.Int. J Biol Macromol 186:770–779. https://doi.org/10.1016/j.ijbiomac.2021.07.097
33. Sarwar MS, Niazi MBK, Jahan Z, Ahmad T, Hussain A (2018) Preparation and characterization of PVA/nanocellulose/Ag nanocomposite films for antimicrobial food packaging. Carbohydr Polym 184:453–464. https://doi.org/10.1016/j.carbpol.2017.12.068
34. Spiridon I, Ursu RG, Spiridon IAC (2015) New Polylactic Acid composites for Packaging Applications: Mechanical properties, Thermal Behavior, and antimicrobial activity. Int J Polym Anal 20(8):681–692. https://doi.org/10.1080/1023666X.2015.1081131
35. Ghozali M, Fahmiati S, Triwulandari E, Restu WK, Farhan D, Wulansari M, Fatriasari W (2020) PLA/metal oxide biocomposites for antimicrobial packaging application. Polym -Plast Technol Mater 59(12):1332–1342. https://doi.org/10.1080/25740881.2020.1738475
36. Szymańska-Chargot M, Chylińska M, Pieczywek PM, Walkiewicz A, Pertile G, Frąc M, Cieślak KJ, Zdunek A (2020) Evaluation of Nanocomposite made of Polylactic Acid and Nanocellulose from Carrot Pomace modified with Silver Nanoparticles. Polymers 12(4):812. https://doi.org/10.3390/polym12040812
37. Fortunati E, Armentano I, Iannoni A, Kenny JM (2010) Development and thermal behaviour of ternary PLA matrix composites. Polym Degrad Stab 95(11):2200–2206. https://doi.org/10.1016/j.polymdegradstab.2010.02.034
38. Jamnongkan T, Jaroensuk O, Khankhuean A, Laobuthee A, Srisawat N, Pangon A, Mongkholrattanasit R, Phuengphai P, Wattanakornsiri A, Huang C-F (2022) A comprehensive evaluation of mechanical, thermal, and Antibacterial properties of PLA/ZnO Nanoflower Biocomposite filaments for 3D Printing Application. Polymers 14(3):600. https://doi.org/10.3390/polym14030600
39. Sucinda EF, Majid A, Ridzuan MS, Cheng MJM, Alshahrani EM, H. A., Mamat N (2021) Development and characterisation of packaging film from Napier cellulose nanowhisker reinforced polylactic acid (PLA) bionanocomposites. Int J Biol Macromol 187:43–53. https://doi.org/10.1016/j.ijbiomac.2021.07.069
40. Jayachandran A et al (2021) Green synthesis and characterization of zinc oxide nanoparticles using *Cayratia pedata* leaf extract. Biochem Biophys Rep. https://doi.org/10.1016/j.bbrep.2021.100995
41. Song JY, Kim BS (2008) Biological synthesis of bimetallic Au/Ag nanoparticles using Persimmon (Diopyros Kaki) leaf extract. Korean J Chem Eng 25(4):808–811. https://doi.org/10.1007/s11814-008-0133-z
42. Sadiq H, Sher F, Sehar S, Lima EC, Zhang S, Iqbal HMN, Zafar F, Nuhanović M (2021) Green synthesis of ZnO nanoparticles from *Syzygium cumini* leaves extract with robust photocatalysis applications. Period Eng Natl Sci. https://doi.org/10.1016/j.molliq.2021.116567
43. Cui C, Gao L, Dai L, Ji N, Qin Y, Shi R, Qiao Y, Xiong L, Sun Q (2023) Hydrophobic Biopolymer-based films: strategies, properties, and Food Applications. Food Eng Rev 15(2):360–379. https://doi.org/10.1007/s12393-023-09342-6
44. Lizundia E, Pérez-Álvarez L, Sáenz-Pérez M, Patrocinio D, Vilas JL, León LM (2016) Physical ageing and mechanical performance of poly(l-lactide)/ZnO nanocomposites. J Appl Polym Sci. https://doi.org/10.1002/app.43619
45. Okeke IS, Agwu KK, Ubachukwu AA, Ezema FI (2022) Influence of transition metal doping on physiochemical and antibacterial properties of ZnO nanoparticles: a review. Appl Surf Sci Adv 8:100227. https://doi.org/10.1016/j.apsadv.2022.100227
46. Abebe B, Zereffa EA, Tadesse A, Murthy HCA (2020) A review on enhancing the antibacterial activity of ZnO: mechanisms and microscopic investigation. Nanoscale Res Lett 15(1):190. https://doi.org/10.1186/s11671-020-03418-6
47. Zhu Y, Gu X, Dong Z, Wang B, Jin X, Chen Y, Cui M, Wang R, Zhang X (2023) Regulation of polylactic acid using irradiation and preparation of PLA–SiO_2–ZnO melt-blown nonwovens for antibacterial and air filtration. RSC Adv 13(12):7857–7866. https://doi.org/10.1039/D2RA08274H
48. Valerini D, Tammaro L, Villani F, Rizzo A, Caputo I, Paolella G, Vigliotta G (2020) Antibacterial Al-doped ZnO coatings on PLA films. J Mater Sci 55(11):4830–4847. https://doi.org/10.1007/s10853-019-04311-z
49. Bhaskar B, Owen R, Bahmaee H, Wally Z, Sreenivasa Rao P, Reilly GC (2018) Composite porous scaffold of PEG/PLA support improved bone matrix deposition *in vitro* compared to PLA-only scaffolds. J Biomed Mater Res A 106(5):1334–1340. https://doi.org/10.1002/jbm.a.36336
50. Wan Z, Wang L, Ma L, Sun Y, Yang X (2017) Controlled hydrophobic biosurface of bacterial cellulose nanofibers through self-assembly of natural Zein Protein. ACS Biomater Sci Eng 3(8):1595–1604. https://doi.org/10.1021/acsbiomaterials.7b00116
51. Nonato RC, Mei LHI, Bonse BC, Chinaglia EF, Morales AR (2019) Nanocomposites of PLA containing ZnO nanofibers made by solvent cast 3D printing: production and characterization. Eur Polym J 114:271–278. https://doi.org/10.1016/j.eurpolymj.2019.02.026
52. Wu T-M, Wu C-Y (2006) Biodegradable poly (lactic acid)/chitosan-modified montmorillonite nanocomposites: Preparation and characterization. Polym Degrad Stab 91(9):2198–2204. https://doi.org/10.1016/j.polymdegradstab.2006.01.004
53. Marra A, Silvestre C, Duraccio D, Cimmino S (2016) Polylactic acid/zinc oxide biocomposite films for food packaging application. Int J Biol Macromol 88:254–262. https://doi.org/10.1016/j.ijbiomac.2016.03.039
54. Ngo TMP, Dang TMQ, Tran TX, Rachtanapun P (2018) Effects of Zinc Oxide nanoparticles on the Properties of Pectin/Alginate Edible Films. Int J Polym Sci 2018:1–9. https://doi.org/10.1155/2018/5645797
55. Suryanegara L, Fatriasari W, Zulfiana D, Anita SH, Masruchin N, Gutari S, Kemala T (2021) Novel antimicrobial bioplastic based on PLA-chitosan by addition of TiO_2 and ZnO. J Environ Health Sci Eng 19(1):415–425. https://doi.org/10.1007/s40201-021-00614-z
56. Shankar S, Wang L-F, Rhim J-W (2018) Incorporation of zinc oxide nanoparticles improved the mechanical, water vapor

barrier, UV-light barrier, and antibacterial properties of PLA-based nanocomposite films. Mater Sci Eng C 93:289–298. https://doi.org/10.1016/j.msec.2018.08.002
57. Murariu M, Doumbia A, Bonnaud L, Dechief A, Paint Y, Ferreira M, Campagne C, Devaux E, Dubois P (2011) High-performance Polylactide/ZnO nanocomposites designed for films and fibers with Special End-Use Properties. Biomacromolecules 12(5):1762–1771. https://doi.org/10.1021/bm2001445
58. Drelich J (2013) Guidelines to measurements of reproducible contact angles using a sessile-drop technique. Surf Innov 1(4):248–254. https://doi.org/10.1680/si.13.00010
59. Rahman MM, Islam MS, Li GS (2018) Development of PLA/CS/ZnO nanocomposites and optimization its mechanical. Therm Water Absorpt Prop Polym Test 68:302–308. https://doi.org/10.1016/j.polymertesting.2018.04.026
60. Silva MRF, Alves MFRP, Cunha JPGQ, Costa JL, Silva CA, Fernandes MHV, Vilarinho PM, Ferreira P (2023) Nanostructured transparent solutions for UV-shielding: recent developments and future challenges. Mater Today Phys 35:101131. https://doi.org/10.1016/j.mtphys.2023.101131
61. Li Y, Li H, Huang J, Huang L, Chen L, Ni Y, Zheng Q (2022) An environmentally friendly and highly transparent ZnO/cellulose nanocomposite membrane for UV sensing and shielding. Cellulose 29(8):4439–4453. https://doi.org/10.1007/s10570-022-04540-7
62. Tripathi S, Kumar L, Deshmukh RK, Gaikwad KK (2023) Ultraviolet blocking films for Food Packaging Applications. Food Bioproc Tech. https://doi.org/10.1007/s11947-023-03221-y
63. Wang B, Jiang F, Ma X, Dong Z, Liu Y (2022) Preparation of highly dispersed ZnO nanoparticles to fabricate ultraviolet-shielding poly (vinyl chloride) films. Colloid Polym Sci 300(1):51–57. https://doi.org/10.1007/s00396-021-04929-z